Biophysical *Journal*
Article

Biophysical Society

Loop extrusion driven volume phase transition of entangled chromosomes

Tetsuya Yamamoto[1,*] and Helmut Schiessel[2]
[1]Institute for Chemical Reaction Design and Discovery, Hokkaido University, Sapporo, Japan and [2]Cluster of Excellence Physics of Life, TU Dresden, Dresden, Germany

ABSTRACT Experiments on reconstituted chromosomes have revealed that mitotic chromosomes are assembled even without nucleosomes. When topoisomerase II (topo II) is depleted from such reconstituted chromosomes, these chromosomes are not disentangled and form "sparklers," where DNA and linker histone are condensed in the core and condensin is localized at the periphery. To understand the mechanism of the assembly of sparklers, we here take into account the loop extrusion by condensin in an extension of the theory of entangled polymer gels. The loop extrusion stiffens an entangled DNA network because DNA segments in the elastically effective chains are translocated to loops, which are elastically ineffective. Our theory predicts that the loop extrusion by condensin drives the volume phase transition that collapses a swollen entangled DNA gel because the stiffening of the network destabilizes the swollen phase. This may be an important piece to understand the mechanism of the assembly of mitotic chromosomes.

SIGNIFICANCE This paper shows that the loop extrusion stiffens entangled chromosomes because DNA segments in elastically effective chains are translocated by condensin to produce loops, which are elastically ineffective. This stiffening effect drives the volume phase transition with which entangled chromosomes collapse discontinuously. This function of loop extrusion by condensin has not been identified. This theory provides the possibility that the DNA condensation at the entry of mitosis is driven by the volume phase transition.

INTRODUCTION

At the entry of mitosis, chromatin, which has been distributed within the nucleus in interphase, is condensed into mitotic chromosomes by metaphase via a series of structural transitions. A mitotic chromosome is composed of two sister chromatids, which are bound at the centromere by cohesin. Each sister chromatid forms a cylindrical structure, where the loops of chromatin are densely packed along the axis. This structure has attracted molecular and cell biologists for more than 160 years (1). A crucial player in the formation of mitotic chromosomes is condensin, a ring-shaped protein complex that is loaded onto DNA by embracing it (2). The loop extrusion theory predicts that the chromatin loops of mitotic chromosomes are produced by condensin via the loop extrusion process, with which chromatin segments are uni-directionally transported from the chromosome axis to the loops (3–6). The loop extrusion activity of condensin was visualized and characterized by using the DNA-curtain technique (7–9). Theoretically, mitotic chromosomes are studied by using the analogy with bottle brush polymers, in which side chains are densely packed along their main chains (10,11).

In recent experiments, Hirano and coworkers have reconstituted mitotic chromosomes (12–14). They showed that condensin and topoisomerase II (topo II) are necessary components to assemble mitotic chromosomes for DNA derived from mouse sperm cells by depleting protamines and nucleosomes (13) (see Fig. 1 *a*). Topo II is an enzyme that disentangles DNA by transiently breaking the double strand and then ligating it (15,16). When both topo II and condensin are depleted, chromosomes behave as swollen entangled networks, failing to be individualized and to form the condensed cylindrical structure (see Fig. 1 *b*). Shintomi and Hirano have recently discovered that when condensin is present and topo II is depleted, DNA forms a new structure, called sparkler (14) (see Fig. 1 *c*). The feature of sparkler is that DNA and histone H1.8 are condensed in the core, and condensin I is excluded to the periphery. The mechanism of the assembly of reconstituted chromosomes have been experimentally studied intensively in recent years (12–14,17,18).

Submitted April 12, 2022, and accepted for publication June 9, 2022.
*Correspondence: tyamamoto@icredd.hokudai.ac.jp
Editor: Lars Nordenskiöld.
https://doi.org/10.1016/j.bpj.2022.06.014

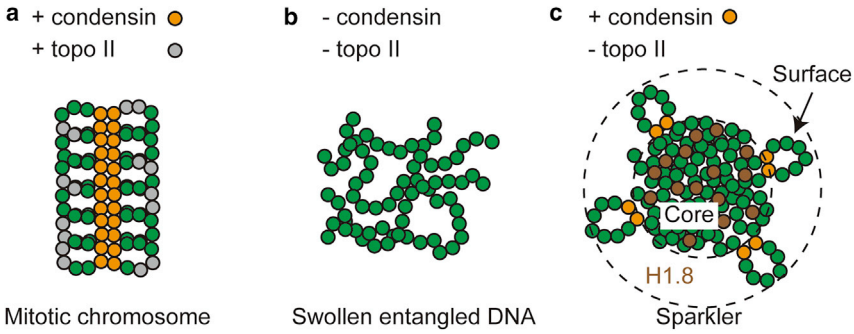

FIGURE 1 Polymorphism of reconstituted chromosomes, from which nucleosomes are removed. (*a*) With condensin and topoisomerase II (topo II), the reconstituted chromosomes form a structure akin to a mitotic chromosome. (*b*) Without condensin and topo II, the reconstituted chromosomes behave as an entangled polymer network. (*c*) When only topo II is depleted, the reconstituted chromosomes form sparklers, where DNA and linker histone H1.8 are condensed in the core and condensin is localized at the periphery. DNA segments, condensin, topo II, and H1.8 are represented by green, orange, gray, and brown circles, respectively. To see this figure in color, go online.

To understand the mechanism of the assembly of sparklers, it is instructive to think of how the loop extrusion by condensin affects the mechanics of entangled DNA networks. In polymer physics, entanglements are treated as effective cross-links that can slide along the chains (these effective cross-links are called slip-links) (19–22). Networks of synthetic polymers are prepared by cross-linking polymers in solution. Network chains that are stretched or shrunken by the deformation of the network contribute to the elasticity of the network and thus are called elastically effective (23,24) (see Fig. 2). Network chains that form loops are not stretched or shrunken by the network deformation and thus are called elastically ineffective. Loop extrusion translocates chromatin segments in the elastically effective fraction of the network to the elastically ineffective loops. Loop extrusion thus stiffens the network by decreasing the number of chromatin segments in the elastically effective fraction of the network. We here take into account the stiffening of the network by the loop extrusion in an extension of the statistical thermodynamic theory of polymer gels to understand the mechanism of the assembly of sparklers. Our theory predicts that entangled DNA networks show a discontinuous transition between swollen and collapsed states—a volume phase transition (25,26)—by changing the loop extrusion activity of condensing.

MATERIALS AND METHODS

Entangled DNA gel

We here construct a minimal model of entangled chromosomes. We treat these chromosomes as very long flexible chains that are not disentangled on the experimental timescale. The chains are assumed to be electrically neutral because the electric fields generated from the electric charges of DNA are screened by salt ions in the solution at the physiological salt concentration (27). The chromosomes are treated as an entangled DNA gel composed of N (Kuhn) segments of length b. In our model, we take into account the entanglements, the loop extrusion process, and the transient association of DNA by linker histone H1.8 (28) in an extension of the theory of polymer gels (29). We use the affine tube model, with which entanglements are treated as effective cross-links that can slide along chains (19,23).

The free-energy density (per unit volume of the final state) of the entangled DNA gel has the form

$$g = g_{\mathrm{ela}} + g_{\mathrm{sol}} + g_{\mathrm{bnd}}, \tag{1}$$

where g_{ela} is the elastic free energy of the network, g_{sol} is the solution free energy that includes the transient association of DNA by linker histones and the mixing free energy between DNA and solvent, and g_{bnd} is the free energy involved in the binding of linker histones to DNA. This free-energy density is a function of the DNA volume fraction ϕ and the occupancy α of linker histones on DNA-binding sites. The loops are produced by the loop extrusion, which is an active process, and are not densely packed at the periphery. These loops thus do not contribute to the free energy of the system.

Without the loop extrusion by condensin, all the segments in the entangled DNA network are elastically effective, and the number of segments N_{e0} between effective cross-links represents the extent of entanglements between the DNA chains. With the loop extrusion process, N_{l} segments are extruded to form loops and become elastically ineffective. The remaining number of segments in the elastically effective part of the network is $N - N_{\mathrm{l}}$. With these loops, the number of segments N_{e} between effective cross-links have the form

$$\frac{N_{\mathrm{e}}}{N_{\mathrm{e0}}} = 1 - \frac{N_{\mathrm{l}}}{N} \tag{2}$$

because the number N/N_{e0} of effective cross-links due to the entanglements is constant. In deriving Eq. 2, we used the fact that the effective cross-links due to the entanglements can slide along the chain to share the load.

The elastic energy density thus has the form

$$g_{\mathrm{ela}} = \frac{3}{2} k_{\mathrm{B}} T \frac{\phi_{\mathrm{eff}}}{b^3 N_{\mathrm{e}}} \frac{N_{\mathrm{e0}}}{N_{\mathrm{e}}} \lambda^2, \tag{3}$$

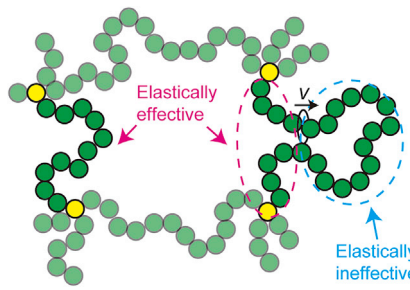

FIGURE 2 Loop extrusion of DNA in an entangled network. In the tube model, the entanglements are represented by effective cross-links (yellow circles). The effective cross-links can slide along the chains with the deformation of the network, and the chains between these cross-links develop tension. These chains contribute to the elastic stress in the network and thus are called elastically effective (see the *magenta broken line*). Loops in the network are not affected by the network deformation. These loops do not contribute to the elastic stress and thus are called elastically ineffective (see the *cyan broken line*). The loop extrusion by condensin (*black circle*) translocates DNA segments (*green circles*) in elastically effective chains to elastically ineffective loops. To see this figure in color, go online.

where the factor N_{e0}/N_e represents the stiffening effect caused by the loop-extrusion process. $\phi_{eff}(=N_e\phi/N_{e0})$ is the volume fraction of elastically effective chains. k_B is the Boltzmann constant, and T is the absolute temperature. λ is the extension ratio with respect to "the reference state" (discussed below). The extension ratios are equal for all the directions because we only treat the swelling and deswelling of the network, and the network is isotropic. In deriving Eq. 3, we use the fact that the number density of "entanglement strands" that are subchains between adjacent effective cross-links is $\phi_{eff}/(b^3N_e)$ and that each entanglement strand contributes an elastic energy of $\frac{3}{2}\frac{k_BT}{\delta R^2}R^2$, where R is the distance between the (time-averaged) positions of the two ends of a subchain and δR is the magnitude of the fluctuation of the subchain (23,24). With the network swelling, each subchain is stretched to $R = \lambda b N_{e0}^{1/2}$, while the magnitude of the fluctuation is $\delta R^2 = b^2N_e$ because the number of segments in the subchain change to N_e due to the loop extrusion process (see above). The extension ratio λ obeys

$$\phi_{eff} = \frac{\phi_0}{\lambda^3}\frac{N_e}{N_{e0}}, \tag{4}$$

which relates the volume fraction ϕ_{eff} of elastically effective chains after the deformation to the DNA volume fraction ϕ_0 at the reference state (see also Eq. 2), accounting for the difference in volume and (effective) monomer numbers between the two states.

The reference state of a synthetic polymer gel is usually taken to the prepared state, where the entanglements are trapped by cross-linking. Instead of treating the entanglement process of mouse sperm chromosomes, which can be complex, we define the reference state as a DNA solution that forms the same number of effective cross-links as the mouse sperm chromosomes. Eq. 3 is rewritten in the form

$$g_{ela} = \frac{3}{2}\frac{G_0}{\lambda^3}\frac{N_{e0}}{N_e}\lambda^2 \tag{5}$$

by introducing the shear modulus $G_0(=k_BT\phi_0/(b^3N_{e0}))$ of the network at the reference state. Fortunately, although the reference state is a gedanken concept, the final result depends on the reference state only via a single parameter $G_0/\phi_0^{1/3}$, which, in principle, is experimentally accessible by measuring the stress-strain relationship of entangled mouse sperm chromosomes.

The solution free energy has the form

$$g_{sol} = \frac{k_BT}{b^3}\left[(1-\phi)\log(1-\phi) - \chi\alpha^2\phi^2\right]. \tag{6}$$

The volume fraction ϕ includes both DNA segments in elastically effective chains and the loops in the core but does not include DNA segments in the loops at the surface. The first term of Eq. 6 is the free-energy contribution of the mixing entropy of DNA and solvent molecules. The second term of Eq. 6 represents the effective interaction due to the transient association of DNA by linker histones, where χ is the corresponding interaction parameter (30) and α is the occupancy of linker histones on DNA-binding sites. This effective interaction represents the tendency for mixtures of DNA and linker histones to phase separate (31,32). Linker histones can be dissociated from DNA-binding sites due to the translocation of the DNA by condensin. With Eq. 6, we treat cases in which the timescale of linker histone binding is shorter than the timescale of the loop extrusion. In the spirit of the affine tube model, we do not take into account the coupling between the transient cross-linking of DNA by linker histone and the entanglement.

The binding free energy has the form

$$g_{bnd} = \frac{k_BT}{b^3}\phi\left[\alpha\log\alpha + (1-\alpha)\log(1-\alpha) + \frac{\varepsilon-\mu}{k_BT}\alpha\right], \tag{7}$$

where ε is the energy due to the binding of linker histones and DNA and μ is the chemical potential of linker histones. Indeed, the interaction parameter has a relationship with the binding energy, $\chi \propto e^{-\varepsilon/(k_BT)}$ (30). The first and second terms of Eq. 7 are the free-energy contribution due to the entropy with respect to the binding of linker histone. The third term of Eq. 7 is the free-energy difference due to the binding of linker histone.

The time evolution of the DNA volume fraction ϕ is governed by the flux of solvent flowing in and out from the entangled DNA gels (29,33–35), and the dynamics of binding between DNA and linker histones determine the occupancy α. In the steady state, the time evolution equations are reduced to the relationships

$$\log\frac{\alpha}{1-\alpha} + \frac{\varepsilon-\mu}{k_BT} - 2\chi\alpha\phi = 0 \tag{8}$$

and

$$\frac{\Pi}{k_BT} = -\frac{G_{e0}b^3}{k_BT}\frac{1}{\lambda}\frac{N_{e0}}{N_e} - \log(1-\phi) - \phi - \chi\alpha^2\phi^2. \tag{9}$$

We used $\frac{\partial g}{\partial\alpha} = 0$ and $\Pi = \phi^2\frac{\partial}{\partial\phi}\left(\frac{g}{\phi}\right)$ to derive Eqs. 8 and 9, respectively. The osmotic pressure Π is constant because there are no fluxes of solvent in the steady state (see refs. (29,33–35)). One has $\Pi = 0$ for cases in which the osmotic pressure at the exterior of the entangled DNA gel is negligible. Eq. 8 implies that linker histones bind to DNA-binding sites due to the binding energy $\varepsilon - \mu$ (the second term) and/or the interaction energy (the third term). The condensation of DNA enhances the binding of linker histone (see the factor ϕ in the third term of Eq. 8). The expression of Eq. 9 is similar to the force balance equation of polymer gels (29,35), except for the stiffening effect due to the loop extrusion process (see the factor N_{e0}/N_e in the first term) and the fact that the attractive interactions between DNA segments are due to linker histones (see the factor α^2 in the fourth term): the volume fraction ϕ is determined by the balance of the elastic stress generated by the DNA network and the osmotic pressure of the solution. We note that the loop extrusion increases the shear modulus of the DNA network, which results from the entropic elasticity of DNA chains and thus shrinks the DNA network. This modulus is different from the osmotic modulus of the whole gel (that includes both of the DNA network and the solvent), which represents the (linear) elastic rigidity against the volume change of the network from the equilibrium swelling (29,35). The DNA volume fraction ϕ and the occupancy α are derived by using Eqs. 8 and 9 once we know the fraction N_{e0}/N_e of elastically ineffective chains, which is determined by the loop extrusion dynamics.

Loop extrusion dynamics

We use an extension of the theory by Goloborodko and coworkers (5) to treat the loop extrusion process. The loop extrusion by condensin is subdivided into the loading process, the translocation process, and the unloading process. For simplicity, we here treat cases in which the loading rate of condensin molecules is relatively small and they do not form nested loops (see also Discussion). Condensin is not loaded to DNA-binding sites that are already bound by linker histones (18) but can be loaded to unoccupied DNA-binding sites with equal probability. In this article, we treat cases in which the concentration of linker histones is relatively small, $\varepsilon - \mu > 0$, and the binding between DNA and linker histones is stabilized by the interaction energy (the third term of Eq. 8). In such cases, the subchains at the core of the gel can be occupied by linker histones as a result of the interaction energy, while the subchains at the surface do not have enough interacting partners to be stably occupied by linker histones. The time evolution equations of the number of condensin at the core, n_c, and at the surface, n_s, have the forms

$$\frac{d}{dt}n_c = k_{on}(1-\gamma_s)N_{eff}(1-\alpha) - \frac{n_c}{\tau_{ex}} \quad (10)$$

and

$$\frac{d}{dt}n_s = k_{on}\gamma_s N_{eff} - \frac{n_s}{\tau_{ex}}, \quad (11)$$

where k_{on} is the loading rate of condensin and is proportional to the concentration of condensin in the solution. τ_{ex} is the average residence time of condensin. γ_s is the ratio of DNA segments at the surface.

In the steady state, the numbers of DNA segments that are already translocated to the loops by condensin at the core, N_c, and at the surface, N_s, have the forms

$$N_c = \frac{1}{2}v_{ex}(f)\tau_{ex}n_c \quad (12)$$

and

$$N_s = \frac{1}{2}v_{ex}(f)\tau_{ex}n_s, \quad (13)$$

where $v_{ex}(f)$ is the number of DNA segments translocated per unit time (the extrusion rate). The factor $1/2$ in Eqs. 12 and 13 represents the fact that the fraction of condensin that has translocated l DNA segments ($0 < l < v_0\tau_{ex}$) is equal at any moment of time in the steady state. The fraction $N_{eff}/N(= 1 - N_l/N)$ of elastically effective chains is derived by using the relationship $N_l = N_c + N_s$ (see also Eq. 2).

In general, the extrusion rate $v_{ex}(f)$ depends on the tension f applied to the DNA. We here use the linear force-velocity relationship

$$v_{ex}(f) = v_0\left(1 - \frac{f}{f_{st}}\right) \quad (14)$$

for $f < f_{st}$ and $v_{ex} = 0$ for $f > f_{st}$, where v_0 is the extrusion rate at $f = 0$ and f_{st} is the stall force, analogous to the treatments for other molecular motors (36). The extrusion rate v_0 and the stall force f_{st} of yeast condensin are in the order of 1.0 kbps ($\sim$ 3 DNA segments per second) and 1 pN, respectively (see the force-velocity relationship in ref. (8)). The processivity $v_0\tau_{ex}$ of condensin I is in the order of 24 kbps ($\sim$ 80 DNA segments) (37). With our model of entangled DNA gels, the tension f has the form

$$\frac{fb}{k_BT} = \frac{3N_{e0}^{1/2}}{N_e}\lambda. \quad (15)$$

Eq. 15 is derived by using the elastic force $f = 3k_BTR/\delta R^2$ of an entanglement strand with $R = \lambda b N_{e0}^{1/2}$ and $\delta R^2 = b^2 N_e$ (see the discussion below Eq. 3).

By solving Eqs. 10 and 11 with respect to n_c and n_s in the steady state, Eqs. 12 and 13 are rewritten in the forms

$$N_c = \frac{\zeta(1-\gamma_s)(1-\alpha)}{1+\zeta((1-\gamma_s)(1-\alpha)+\gamma_s)}N \quad (16)$$

and

$$N_s = \frac{\zeta\gamma_s}{1+\zeta((1-\gamma_s)(1-\alpha)+\gamma_s)}N \quad (17)$$

with

$$\zeta = \frac{1}{2}k_{on}v_{ex}(f)\tau_{ex}^2. \quad (18)$$

Because ζ is a function of the tension f, we define a parameter

$$\zeta_0 = \frac{1}{2}k_{on}v_0\tau_{ex}^2, \quad (19)$$

which represents the extent of the loop extrusion activity for $f = 0$.

RESULTS

The DNA volume fraction ϕ and the occupancy α of linker histones of the entangled DNA gel are derived by using Eqs. 8 and 9 as functions of 6 parameters: the loop extrusion activity ζ_0, the chemical potential of linker histones $(\mu - \varepsilon)/(k_BT)$, the interaction parameter χ, the stall force $f_{st}b/(k_BT)$ of condensin, the shear modulus $G_0b^3/(k_BT\phi_0^{1/3})$ at the reference state, and the fraction γ_s of strands at the surface. One can change the loop extrusion activity ζ_0 and the chemical potential μ of linker histones by changing the concentrations of condensin and linker histones. Eq. 8 has two stable solutions and one unstable solution of the occupancy α for $\mu_{th1} < \mu < \varepsilon - 2k_BT$. The threshold chemical potential μ_{th1} depends only on the interaction parameter χ and has the analytical form

$$\frac{\varepsilon - \mu_{th1}}{k_BT} = \frac{2}{1-\sqrt{1-2/\chi}} - \log\frac{1+\sqrt{1-2/\chi}}{1-\sqrt{1-2/\chi}} \quad (20)$$

(see the cyan dot in Fig. 3). Eq. 20 is derived by the conditions $(\varepsilon - \mu)/(k_BT) \geq 2$, $\phi = 1$ and $\frac{\partial}{\partial\alpha}(2\chi\phi) = 0$, with which Eq. 8 has multiple solutions (see Section S1). The occupancy α is derived as the stable solution with the smaller free energy g/ϕ. In general, the tension developed in the

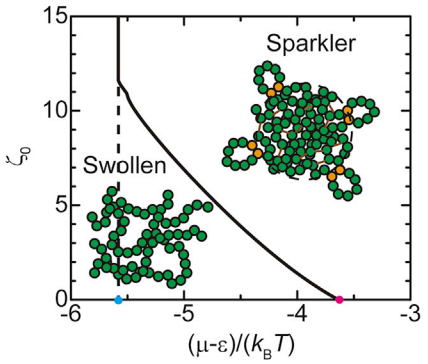

FIGURE 3 The phase diagram of an entangled DNA gel with respect to the loop extrusion activity ζ_0 and the chemical potential μ of linker histones for $f_{st} \to \infty$. The cyan and magenta dots are the two threshold values, μ_{th1} and μ_{th2}, of the chemical potential. The loop extrusion activity ζ_0 is defined by Eq. 19. The numerical calculations are performed by using $\chi = 4.3$, $G_0b^3/(k_BT\phi_0^{1/3}) = 0.1$, and $\gamma_s = 0.1$. To see this figure in color, go online.

chromosome can decelerate the loop extrusion of condensin. However, the essential feature of the system is captured even for the simple case that the stall force of condensin is very large, $f_{st} \to \infty$, and the deceleration of the loop extrusion by the tension is negligible, $\zeta = \zeta_0$. We first treat such case in this section.

Without the loop extrusion by condensin, $\zeta_0 = 0$, the entangled DNA gel is swollen for the concentrations of linker histones in the solution smaller than a threshold value, $\mu < \mu_{th2}$, whereas it collapses for $\mu > \mu_{th2}$ (see the *magenta dot* in Fig. 3). The chemical potential μ_{th2} has the asymptotic form

$$\frac{\mu_{th2} - \varepsilon}{k_B T} = 1 - \chi + \frac{3}{2}\frac{G_0 b^3}{k_B T \phi_0^{1/3}} - \frac{5}{4}\left(\frac{G_0 b^3}{k_B T \phi_0^{1/3}}\right)^{3/5} \quad (21)$$

for small shear modulus, $G_0 b^3/(k_B T \phi_0^{1/3}) \approx 0$, large interaction parameter, $\chi \gg 1$, and small chemical potential, $(\mu - \varepsilon)/(k_B T) \ll -1$. For this limiting case, one can assume $\alpha < 1$ and $\phi < 1$ for the swollen phase and $\alpha \approx 1$ and $\phi \approx 1$ for the collapsed phase. Eq. 21 is derived by using the asymptotic expression of the free energy f/ϕ of the two phases for this limit and by finding the condition with which the values of the free energy f/ϕ of the two phases are equal (see Section S2).

The entangled DNA network is swollen for the loop-extrusion activity smaller than a threshold, $\zeta_0 < \zeta_{0th}$ (see Fig. 3). For $\zeta_0 < \zeta_{0th}$, the DNA volume fraction ϕ increases with increasing the loop extrusion activity ζ_0, while the occupancy α is very small and approximately constant (see the *magenta* and *cyan lines* in Fig. 4). The number of DNA segments N_c extruded to the loops in the core also increases with increasing the loop extrusion activity ζ_0 (see the *black line* in Fig. 4). In the swollen phase, the

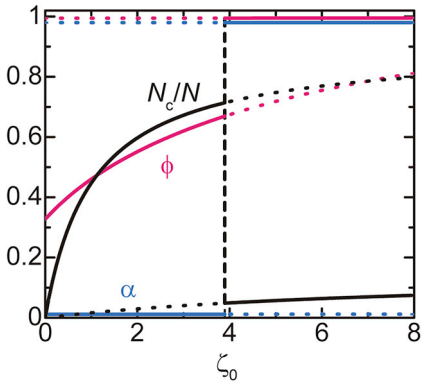

FIGURE 4 The volume phase transition of the entangled DNA gel. The volume phase transition ϕ (*magenta*), the occupancy α of DNA binding sites by linker histones (*cyan*), and the fraction N_c/N of chain segments in the loops at the core (*black*) are shown as a function of the loop extrusion activity ζ_0 (defined by Eq. 19). These curves are derived by using $\chi = 4.3$, $(\mu - \varepsilon)/(k_B T) = -4.5$, and $G_0 b^3/(k_B T \phi_0^{1/3}) = 0.1$, $\gamma_s = 0.1$. To see this figure in color, go online.

DNA volume fraction ϕ and the number of DNA segments N_c in the core have asymptotic forms

$$\phi = \left(\frac{2G_0 b^3}{k_B T \phi_0^{1/3}}\right)^{3/5} \frac{(1+\zeta_0)^{4/5}}{(1+(1-\gamma_s)\zeta_0)^{1/5}} \quad (22)$$

and

$$\frac{N_c}{N} = (1-\gamma_s)\frac{\zeta_0}{1+\zeta_0} \quad (23)$$

for small values of $G_0 b^3/(k_B T \phi_0^{1/3})$. These asymptotic forms are derived by expanding Eqs. 8 and 9 in a power series of α and ϕ and by neglecting higher-order terms (see Section S2.1).

At the threshold loop extrusion activity, $\zeta_0 = \zeta_{0th}$, both the occupancy α and the DNA volume fraction ϕ jump to approximate unity (see the *cyan* and *magenta lines* in Fig. 4), while the number N_c of DNA segments extruded to the loops in the core jumps to a smaller value (see the *black line* in Fig. 4). The jump of the DNA volume fraction ϕ is analogous to the volume phase transition of polymer gels (25,26,35). The volume phase transition is driven by the loop extrusion by condensin: the swollen state is destabilized by the stiffening of the entangled DNA network due to the loop extrusion process and drives the transition to the collapsed state. The collapsed state is stabilized by the transient cross-linking of DNA by linker histones, where the binding of linker histones to DNA, in turn, is enhanced as the concentration of DNA increases (see the third term of Eq. 8). This mechanism is very different from the volume-phase transition of polymer gels in the thermodynamic equilibrium, where the transition is driven by the osmotic pressure of counterions (17) or the cooperative hydration (38). The small number N_c of DNA segments extruded to the loop in the core results from the fact that the loading of condensin to the DNA segments in the core is suppressed by the linker histones bound to these segments (see the *black line* in Fig. 4 and Eq. 16). Condensin is localized at the surface of the entangled DNA network. The features of the entangled DNA network in the collapsed phase are analogous to sparklers. Our theory thus predicts that sparklers are assembled by the volume phase transition of entangled chromosomes.

Now, we take into account the deceleration of loop extrusion by the tension developed in the DNA. The volume-phase transition of the entangled DNA gel is driven by changing the loop extrusion activity ζ_0 for a window $\mu'_{th1} < \mu < \mu_{th2}$ of the chemical potential of linker histones, as in the case of $f_{st} \to \infty$ (see Fig. 5). There are two features that are different from the case of $f_{st} \to \infty$: First, the width $\mu_{th2} - \mu'_{th1}$ of the window of the chemical potential decreases with decreasing the stall force (see Fig. 6). Second, the entangled DNA gel experiences a reentrant transition

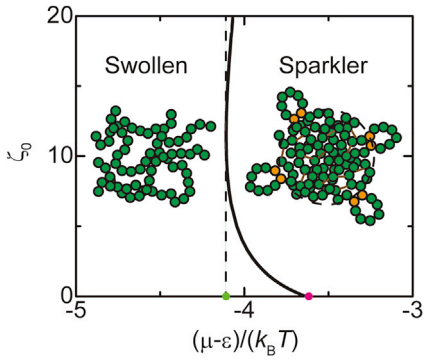

FIGURE 5 The phase diagram of an entangled DNA gel with respect to the loop extrusion activity ζ_0 and the chemical potential μ of linker histones for $f_{st}b/(k_BT) = 5.0$. The light green and magenta dots are the two threshold values, μ_{th1}' and μ_{th2}, of the chemical potential. The loop extrusion activity ζ_0 is defined by Eq. 19. The numerical calculations are performed by using $\chi = 4.3$, $G_0b^3/(k_BT\phi_0^{1/3}) = 0.1$, and $\gamma_s = 0.1$. To see this figure in color, go online.

from the collapsed phase to the swollen phase by increasing the loop extrusion activity ζ_0 to higher values (see Fig. 5). These features imply that the sparkler phase is destabilized by the deceleration of the loop extrusion process. The reentrant volume phase transition results from the fact that the condensin is stalled at a smaller loop extrusion activity ζ_0 in the swollen phase than in the collapsed phase (see factor λ in Eq. 15): the free energy of the collapsed phase increases with increasing the loop extrusion activity, while the free energy of the swollen phase, in which condensin stalls, is constant. The reentrant transition happens when the free energy of the collapsed phase becomes larger than the free energy of the swollen phase.

DISCUSSION

We have constructed a minimal model for reconstituted chromosomes, from which topo II is depleted. The reconstituted chromosomes behave as swollen entangled DNA gels if condensin is depleted. The main concept delineated by this theory is that the loop extrusion by condensin translocates DNA segments from the elastically effective chains of the entangled DNA network to the elastically ineffective chains and thus stiffens the entangled DNA network. The stiffening by the loop extrusion process destabilizes the swollen phase and drives the volume phase transition to the collapsed phase. The collapsed phase is stabilized by the transient cross-linking of DNA by linker histones, where the binding of linker histones to DNA is, in turn, enhanced by the condensation of DNA. This mechanism of the volume phase transition is very different from the classical mechanisms, such as the osmotic pressure of counterions (17) and cooperative hydration (38).

Our theory predicts that DNA and linker histones are condensed at the core of the entangled DNA network, while condensin is excluded from the core and acts mainly at the surface of the network. These predicted features of the collapsed phase are analogous to the sparklers found by Shintomi and Hirano (14). Our theory predicts that the effective attractive interactions due to the transient cross-linking between DNA segments by linker histone drive the condensation of DNA and that linker histone at the core suppresses the loading of condensin to these segments. The sparklers typically have a couple of protrusions (14). These protrusions may result from the adhesion of condensin at the surface to the cover slip and are beyond the scope of our theory. Comparison with mitotic chromosomes *in vivo* is more challenging because chromosomes are already individualized in the early prophase (39). The volume phase transition may be involved in mutants, from which topo II depleted, and/or at the short timescale before chromosomes are individualized by topo II.

Estimating the values of parameters involved in our theory may be useful to experimentally test our theory. The processivity $v_0\tau_{ex}$ of condensin I is in the order of 24 kbps, which corresponds to $\sim$ 80 DNA segments (37). For cases in which the number of condensin loaded on DNA is one every 10 segments, $\frac{n_s+n_c}{N_{eff}} = k_{on}\tau_{ex} \approx 0.1$, in the steady state, the loop-extrusion activity ζ_0 defined by Eq. 19 can be estimated as ≈ 4. The loop extrusion activity ζ_0 is proportional to the concentration of condensin in the solution and thus can be controlled experimentally. The chemical potential $\mu/(k_BT)$ is the logarithm of the volume fraction of linker histones and is another quantity that can be controlled experimentally. The chemical potential is $\mu/(k_BT) \approx -12$ for cases in which the concentration of linker histone is ≈ 100 nM by roughly estimating the volume of a linker histone as 100 nm^3 (40). It is harder to estimate the binding energy $\varepsilon/(k_BT)$ because the dissociation rate of linker histone depends on histone chaperone Nap1 (28). The interaction parameter χ is widely used to represent the magnitude of the interactions between polymers in a solution (23). One can use the relationship $\chi \propto e^{-\varepsilon/(k_BT)}$ to estimate the interaction parameter χ (30), but the value of the binding energy is necessary. The interaction parameter χ may be experimentally accessible, independently from the binding energy, by measuring the radius of gyration of DNA as a function of the concentration of linker histone (and Nap1) *in vitro* (41). It is also difficult to estimate the elastic modulus $G_0b^3/(k_BT\phi_0^{1/3})$ of entangled chromosomes because of the lack of information on the extent of the entanglement between an entangled chromosomes used in the reconstituted system and the quantitative relationship between the extent of the entanglement, and the number N_{e0} of segments in an entanglement strand remains to be identified. This quantity, however, can be, in principle, extracted from the measurements of the stress-strain relationship of the chromosomes. The asymptotic expressions of the occupancy α, the DNA volume fraction ϕ, and the number N_c of DNA segments in the loops shown in Section S2 may be useful to quantitatively test our theory in future experiments.

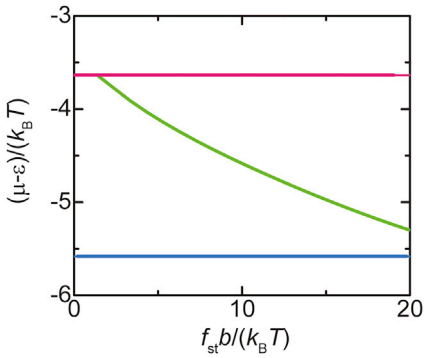

FIGURE 6 The threshold chemical potentials μ_{th1} (*cyan*), μ_{th1}' (*light green*), and μ_{th2} (*magenta*) versus the stall force f_{st}. The numerical calculations are performed by using $\chi = 4.3$, $G_0b^3/(k_BT\phi_0^{1/3}) = 0.1$, and $\gamma_s = 0.1$. To see this figure in color, go online.

Our model takes into account the deceleration of the loop extrusion by the tension developed in the DNA. The deceleration mechanism can be significant in entangled DNA gels, where the tension developed in DNA does not relax due to the entanglements. This is in contrast to the situation of DNA freely diffusing in a solution (42). The stall force of yeast condensin is reported to be on the order of 1 pN, corresponding to $f_{st}b/(k_BT) \approx 24$ (8). Whether the deceleration mechanism is significant or not depends on the shear modulus $G_0b^3/(k_BT\phi_0^{1/3})$ of the entangled DNA network.

We used a couple of assumptions to simplify the model. First, we treated cases in which the concentration of condensin in the solution is relatively small and assumed that condensin is not loaded to DNA loops that have been already translocated by previously loaded condensin. However, this assumption is not essential for our treatment: in the other limit of large condensin concentrations, the DNA segments that were translocated to the loops return to the elastically effective chains when condensin is unloaded but are soon translocated to the loops by other condensin. Such cases can be treated by using the same formalism but without the factor $1/2$ in Eqs. 12 and 13. Second, we assumed a reference state, a DNA solution that forms the same number of effective cross-links by entanglements as the mouse sperm chromosomes. Such a reference state surely exists for cases in which chromosomes are relaxed to the thermodynamic equilibrium before topo II is depleted. However, it is not trivial whether the reference state exists in general. Our assumption is probably the best given our current knowledge of the polymer entanglement and its simplicity. Third, we neglected the fact that condensin and/or linker histone that are not bound to the DNA network may be excluded from the network due to the excluded volume interaction between these proteins and DNA. Indeed, the osmotic pressure generated by these proteins is constant and does not contribute to the force balance in an open system (see also Section S3 and the discussion in the second paragraph of the conclusion). Fourth, we assumed a linear relationship between the extrusion rate of condensin and the DNA tension (see Eq. 14). The functional form of the force-velocity relationship probably influences the details of the boundary between the swollen and collapsed phases. However, we expect that it does not change the essential feature of the system (see also Figs. 3 and 5).

CONCLUSION

The main prediction of our theory is the volume phase transition of entangled chromosomes, which will be observed when one changes the concentration of condensin for a window of the chemical potential of linker histones (see the phase diagram in Fig. 5). This prediction may be experimentally accessible on reconstituted chromosomes, from which topo II is depleted, by changing the concentration of condensin and linker histones. The stiffening of entangled chromosomes due to the loop extrusion may be more directly tested by measuring the stress-strain curve of entangled chromosomes by changing the concentration of condensin in the system.

The volume phase transition of gels of synthetic polymers is a very slow process. However, the volume phase transition of chromosomes can be fast because the chromosomes, which are on the order of micrometer, are smaller than typical synthetic polymer gels, and the mesh size is likely to be rather large. It is therefore tempting to think that the volume phase transition driven by the loop extrusion process is involved in the condensation of chromosomes at the entry of mitosis. Beel and coworkers recently proposed a similar view but with the volume phase transition due to the osmotic pressure of counterions (17). This and our theories are not mutually exclusive. Indeed, our theory predicts the bistability of the swollen and sparkler phases but does not predict the instability of each phase (see Fig. 4). We assume that the volume phase transition can be driven by thermal fluctuations, but the osmotic pressure of counterions or that due to excluded volume interactions between DNA and other molecules, such as condensin and linker histones diffusing in the solution, may result in the instability. Chromosomes can collapse due to the osmotic pressure difference generated by proteins excluded from the chromosomes (43). In the reconstituted system, linker histones are rather localized at the core of the sparkler. Condensin is excluded from the core. However, the concentration of condensin is in the order of 10 nM and thus does not significantly change the osmotic pressure at the exterior (see also the discussion in Section S3).

The dynamics of the structural transition at the entry and exit of mitosis by taking into account the volume phase transition or the disentanglement by topo II will be the subject of our future research. Our theory also provides insight into the mechanism of the assembly of the reconstituted chromosomes, which have been studied intensively in recent years (12–14,17,18).

The mathematica file used for the numerical calculations is available in figshare with the identifier https://doi.org/10.6084/m9.figshare.19882501.

SUPPORTING MATERIAL

Supporting material can be found online at https://doi.org/10.1016/j.bpj.2022.06.014.

AUTHOR CONTRIBUTIONS

T.Y. designed the research, constructed the model, carried out all the numerical calculations, and derived asymptotic analytical results. H.S. proposed the mechanism of the formation of the protrusions observed from sparklers. T.Y. and H.S. wrote and revised the manuscript.

ACKNOWLEDGMENTS

This work was supported by JSPS KAKENHI grant numbers 20H05934 (Genome Modality), 21K03479, and 21H00241. T.Y. acknowledges discussions with T. Hirano (Riken), K. Shintomi (Riken), H. Niki (National Institute for Genetics), A. Kimura (National Institute for Genetics), and T. Sakaue (Aoyama Gakuin). H.S. was supported by the Deutsche Forschungsgemeinschaft (DFG; German Research Foundation) under Germany's Excellence Strategy – EXC-2068 – 390729961.

DECLARATION OF INTERESTS

The authors declare no competing interests.

REFERENCES

1. Paulson, J. R., D. F. Hudson, …, W. C. Earnshaw. 2021. Mitotic chromosomes. *Semin. Cell Dev. Biol.* 117:7–29. https://doi.org/10.1016/j.semcdb.2021.03.014.
2. Hirano, T. 2016. Condensin-based chromosome organization from bacteria to vertebrates. *Cell.* 164:847–857. https://doi.org/10.1016/j.cell.2016.01.033.
3. Alipour, E., and J. F. Marko. 2012. Self-organization of domain structures by DNA-loop-extruding enzymes. *Nucleic Acids Res.* 40:11202–11212. https://doi.org/10.1093/nar/gks925.
4. Naumova, N., M. Imakaev, …, J. Dekker. 2013. Organization of the mitotic chromosome. *Science.* 342:948–953. https://doi.org/10.1126/science.1236083.
5. Goloborodko, A., J. Marko, and L. Mirny. 2016. Chromosome compaction by active loop extrusion. *Biophys. J.* 110:2162–2168. https://doi.org/10.1016/j.bpj.2016.02.041.
6. Goloborodko, A., M. V. Imakaev, …, L. Mirny. 2016. Compaction and segregation of sister chromatids via active loop extrusion. *Elife.* 5:e14864. https://doi.org/10.7554/elife.14864.
7. Terakawa, T., S. Bisht, …, E. C. Greene. 2017. The condensin complex is a mechanochemical motor that translocates along DNA. *Science.* 358:672–676. https://doi.org/10.1126/science.aan6516.
8. Ganji, M., I. A. Shaltiel, …, C. Dekker. 2018. Real-time imaging of DNA loop extrusion by condensin. *Science.* 360:102–105. https://doi.org/10.1126/science.aar7831.
9. Golfier, S., T. Quail, …, J. Brugués. 2020. Cohesin and condensin extrude DNA loops in a cell cycle-dependent manner. *Elife.* 9:e53885. https://doi.org/10.7554/elife.53885.
10. Gibcus, J. H., K. Samejima, …, J. Dekker. 2018. A pathway for mitotic chromosome formation. *Science.* 359:eaao6135. https://doi.org/10.1126/science.aao6135.
11. Brahmachari, S., and J. F. Marko. 2019. Chromosome disentanglement driven via optimal compaction of loop-extruded brush structures. *Proc. Nat. Acad. Sci. U S A.* 116:24956–24965. https://doi.org/10.1073/pnas.1906355116.
12. Shintomi, K., T. S. Takahashi, and T. Hirano. 2015. Reconstitution of mitotic chromatids with a minimum set of purified factors. *Nat. Cell Biol.* 17:1014–1023. https://doi.org/10.1038/ncb3187.
13. Shintomi, K., F. Inoue, …, T. Hirano. 2017. Mitotic chromosome assembly despite nucleosome depletion in Xenopus egg extracts. *Science.* 356:1284–1287. https://doi.org/10.1126/science.aam9702.
14. Shintomi, K., and T. Hirano. 2021. Guiding functions of the C-terminal domain of topoisomerase IIα advance mitotic chromosome assembly. *Nat. Commun.* 12:2917. https://doi.org/10.1038/s41467-021-23205-w.
15. Nitiss, J. L. 2009. DNA topoisomerase II and its growing repertoire of biological functions. *Nat. Rev. Cancer.* 9:327–337. https://doi.org/10.1038/nrc2608.
16. Pommier, Y., Y. Sun, …, J. L. Nitiss. 2016. Roles of eukaryotic topoisomerases in transcription, replication and genomic stability. *Nat. Rev. Mol. Cell Biol.* 17:703–721. https://doi.org/10.1038/nrm.2016.111.
17. Beel, A. J., P. J. Mattei, and R. D. Kornberg. 2021. Mitotic chromosome condensation driven by a volume phase transition. Preprint at bioRxiv. https://doi.org/10.1101/2021.07.30.454418.
18. Choppakatla, P., B. Dekker, …, H. Funabiki. 2021. Linker histone H1.8 inhibits chromatin-binding of condensins and DNA topoisomerase II to tune chromosome length and individualization. *Elife.* 10:e68918. https://doi.org/10.7554/elife.68918.
19. Edwards, S. F. 1967. The statistical mechanics of polymerized material. *Proc. Phys. Soc.* 92:9–16. https://doi.org/10.1088/0370-1328/92/1/303.
20. Ball, R., M. Doi, …, M. Warner. 1981. Elasticity of entangled networks. *Polymer.* 22:1010–1018. https://doi.org/10.1016/0032-3861(81)90284-6.
21. Masubuchi, Y., and T. Uneyama. 2019. Retardation of the reaction kinetics of polymers due to entanglement in the post-gel stage in multi-chain slip-spring simulations. *Soft Matter.* 15:5109–5115. https://doi.org/10.1039/c9sm00681h.
22. Masubuchi, Y. 2021. Elasticity of randomly cross-linked networks in primitive chain network simulations. *Nihon Reoroji Gakkaishi.* 49:73–78. https://doi.org/10.1678/rheology.49.73.
23. Rubinstein, M., and R. H. Colby. 2003. Polymer Physics. Oxford University Press.
24. Yamamoto, T., J. A. Campbell, …, M. Rubinstein. 2022. Scaling theory of swelling and deswelling of polymer networks. *Macromolecules.* 55:3588–3601. https://doi.org/10.1021/acs.macromol.1c02553.
25. Hirokawa, Y., and T. Tanaka. 1984. Volume phase transition in a nonionic gel. *J. Chem. Phys.* 81:6379–6380. https://doi.org/10.1063/1.447548.
26. Tanaka, T., E. Sato, …, J. Peetermans. 1985. Critical kinetics of volume phase transition of gels. *Phys. Rev. Lett.* 55:2455–2458. https://doi.org/10.1103/physrevlett.55.2455.
27. Marko, J. F., and E. D. Siggia. 1995. Stretching DNA. *Macromolecules.* 28:8759–8770. https://doi.org/10.1021/ma00130a008.
28. Yue, H., H. Fang, …, T. H. Lee. 2016. Single-molecule studies of the linker histone H1 binding to DNA and the nucleosome. *Biochemistry.* 55:2069–2077. https://doi.org/10.1021/acs.biochem.5b01247.
29. Doi, M. 2013. Soft Matter Physics. Oxford University Press.
30. Semenov, A. N., and M. Rubinstein. 1998. Thermoreversible gelation in solutions of associative polymers. 1. Statics. *Macromolecules.* 31:1373–1385. https://doi.org/10.1021/ma970616h.
31. Gibson, B. A., L. K. Doolittle, …, M. K. Rosen. 2019. Organization of chromatin by intrinsic and regulated phase separation. *Cell.* 179:470–484.e21. https://doi.org/10.1016/j.cell.2019.08.037.

32. Turner, A. L., M. Watson, …, K. Stott. 2018. Highly disordered histone H1-DNA model complexes and their condensates. *Proc. Nat. Acad. Sci. U S A.* 115:11964–11969. https://doi.org/10.1073/pnas.1805943115.

33. Tomari, T., and M. Doi. 1994. Swelling dynamics of a gel undergoing volume transition. *J. Phys. Soc. Jpn.* 63:2093–2101. https://doi.org/10.1143/jpsj.63.2093.

34. Tomari, T., and M. Doi. 1995. Hysteresis and incubation in the dynamics of volume transition of spherical gels. *Macromolecules.* 28:8334–8343. https://doi.org/10.1021/ma00128a050.

35. Doi, M. 2009. Gel dynamics. *J. Phys. Soc. Jpn.* 78:052001. https://doi.org/10.1143/jpsj.78.052001.

36. Korn, C. B., S. Klumpp, …, U. S. Schwarz. 2009. Stochastic simulations of cargo transport by processive molecular motors. *J. Chem. Phys.* 131:245107. https://doi.org/10.1063/1.3279305.

37. Kong, M., E. E. Cutts, …, E. C. Greene. 2020. Human condensin I and II drive extensive ATP-dependent compaction of nucleosome-bound DNA. *Mol. Cell.* 79:99–114.e9. https://doi.org/10.1016/j.molcel.2020.04.026.

38. Kojima, H., and F. Tanaka. 2010. Cooperative hydration induces discontinuous volume phase transition of cross-linked poly(*N*-isopropylacrylamide) gels in water. *Macromolecules.* 43:5103–5113. https://doi.org/10.1021/ma100588f.

39. Kireeva, N., M. Lakonishok, …, A. S. Belmont. 2004. Visualization of early chromosome condensation: a hierarchical folding, axial glue model of chromosome structure. *J. Cell Biol.* 166:775–785. https://doi.org/10.1083/jcb.200406049.

40. Fyodorov, D. V., B. R. Zhou, …, Y. Bai. 2018. Emerging roles of linker histones in regulating chromatin structure and function. *Nat. Rev. Mol. Cell Biol.* 19:192–206. https://doi.org/10.1038/nrm.2017.94.

41. Oohashi, T., K. Inoue, and Y. Nakamura. 2014. Second and third virial coefficients of low-molecular-weight polyisoprene in 1, 4-dioxane. *Polym. J.* 46:699–703. https://doi.org/10.1038/pj.2014.43.

42. Yamamoto, T., T. Sakaue, and H. Schiessel. 2019. Loop extrusion drives very different dynamics for Rouse chains in bulk solutions and at interfaces. *Europhys. Lett.* 127:38002. https://doi.org/10.1209/0295-5075/127/38002.

43. de Vries, R. 2010. DNA condensation in bacteria: interplay between macromolecular crowding and nucleoid proteins. *Biochimie.* 92:1715–1721. https://doi.org/10.1016/j.biochi.2010.06.024.